# ON THE CALCULATION OF DOME-TRANSDUCER INTERACTIONS FOR A NONLINEAR PARAMETRIC SONAR

Boyd B. Cary, et al

TRACOR, Incorporated

Prepared for:

Naval Ship Systems Command

6 November 1973

Contract N00024-73-C-1131
Tracor Project 025-004
Document Number T-73-NJ-4005-U



FINAL REPORT

# ON THE CALCULATION OF DOME-TRANSDUCER INTERACTIONS FOR A NONLINEAR PARAMETRIC SONAR (U)

Project No. 11121601 Task No. 16833

Submitted to

Naval Ship Systems Command

Department of the Navy

Washington, D.C. 20360

Attention: SHIPS PMS 302-412



6 November 1973

TRACOR

50 EVERGREEN PLACE/EAST ORANGE, NEW JERSEY 07018/AC 201-672-5600/TWX 710-994-5828
HOME OFFICE: TRACOR INC., 6500 TRACOR LANE, AUSTIN, TEXAS 78721, AC 512-926-2800

Unclassified

Security Classification

**DOCUMENT CONTROL DATA - R & D**

*(Security classification of title, body of abstract and indexing annotation must be entered when the overall report is classified)*

1. ORIGINATING ACTIVITY (Corporate author)

Tracor, Inc.
7 Glenwood Avenue
East Orange, N.J. 07017

2a. REPORT SECURITY CLASSIFICATION

unclassified

2b. GROUP

-

3. REPORT TITLE

On the Calculation of Dome-Transducer Interactions for a Nonlinear Parametric Sonar

4. DESCRIPTIVE NOTES (Type of report and inclusive dates)

Final Report

5. AUTHOR(S) (First name, middle initial, last name)

Boyd B. Cary
Bruce Hamilton

| 6. REPORT DATE | 7a. TOTAL NO. OF PAGES | 7b. NO. OF REFS |
|---|---|---|
| 6 November 1973 | ~~36~~ 47 | 3 |

| 8a. CONTRACT OR GRANT NO. | 9a. ORIGINATOR'S REPORT NUMBER(S) |
|---|---|
| N00024-73-C-1131 | T-73-NJ-4005-U |
| 8b. PROJECT NO. 11121601 | |
| 8c. | 9b. OTHER REPORT NO(S) (Any other numbers that may be assigned this report) |
| 8d. | |

10. DISTRIBUTION STATEMENT

None

| 11. SUPPLEMENTARY NOTES | 12. SPONSORING MILITARY ACTIVITY |
|---|---|
| | Naval Ship Systems Command<br>Department of the Navy<br>Washington, D.C. 20360<br>SHIPS PMS 302-412 |

13. ABSTRACT

This study was undertaken in order to extend previously developed computational methods for conventional dome-transducer interactions to the nonlinear parametric case. A simple model involving planar geometry was analyzed in detail in order to gain insight into the sensitivity of parametric generation efficiency to variations in such parameters as steering angle, dome-transducer spacing, and dome thickness. A prescription is given for calculating the interaction for realistic geometries.

DD FORM 1 NOV 65 1473

Security Classification

| 14. KEY WORDS | LINK A | | LINK B | | LINK C | |
|---|---|---|---|---|---|---|
| | ROLE | WT | ROLE | WT | ROLE | WT |
| Parametric Sonar<br>Dome Interaction | | | | | | |

TRACOR

TABLE OF CONTENTS

TRACOR

## ABSTRACT

This study was undertaken in order to extend previously developed computational methods for conventional dome-transducer interactions to the nonlinear parametric case. A simple model involving planar geometry was analyzed in detail in order to gain insight into the sensitivity of parametric generation efficiency to variations in such parameters as steering angle, dome-transducer spacing, and dome thickness. A prescription is given for calculating the interaction for realistic geometries.

TRACOR

## LIST OF ILLUSTRATIONS

TRACOR

LIST OF ILLUSTRATIONS - Continued



LIST OF TABLES

# LIST OF SYMBOLS

| | |
|---|---|
| $V$ | velocity amplitude |
| $k$ | wave number |
| $x,y$ | rectangular coordinates |
| $\omega$ | angular frequency |
| $P$, $p$, $P^*$ | pressure, * indicates complex conjugate |
| $\rho$ | density of fluid |
| $u$ | plate displacement from equilibrium |
| $t$ | time |
| $d$ | dome transducer spacing |
| $\rho_s$ | plate density |
| $h$ | plate thickness |
| $\sigma = \rho_s h$ | |
| $E$ | Young's modulus |
| $\nu$ | Poisson's ratio |
| $\theta$ | steering angle |
| $K = k \sin\theta$ | |
| $\eta = k \cos\theta$ | |

TRACOR

$I_o$ average intensity passing through dome

$D = \imath\eta \left[ e^{-i\eta d} + \frac{\eta}{\omega^2 \rho} \left( -\sigma\omega^2 + HK^4 \right) \sin \eta d \right]$

$H = \frac{Eh^3}{12(1-\nu^2)}$

$T = I_o / I_o$ (with no dome)

$\nabla^2$ Laplace operator

$\beta$ fluid nonlinearity parameter (for sea water $\beta \doteq 3.8$)

$c_o$ small signal sound speed in fluid

$\Gamma$ Green's function

$r, \phi$ polar coordinates of field point

$r_o, \psi$ polar coordinates of virtual source point of the difference frequency field

$R, R_o$ distance to field point from source and its image respectively

$a$ small signal attenuation coefficient

$m = \omega_2 / \omega_1$

$\omega_- = \omega_2 - \omega_1$

$$G = \frac{\beta V_o k_1}{a_1 c_o}$$

$$A = \frac{\beta P_o k_-^{3/2} \omega_1 \omega_2 \sqrt{2\pi}\ e^{i\left(\frac{\pi}{4} - dk_- \cos\theta\right)}}{\rho_o c_o^4 D_1 D_2}$$

$$z = \frac{r_o \sin\psi}{\sin\theta}$$

n summation index

$C_L$ longitudinal wave velocity inside the dome

$C_S$ shear wave velocity inside the dome

TRACOR

## 1.0 INTRODUCTION

In the past Tracor[1] has developed computer programs which allow predictions to be made of the influence of a dome upon the radiated field patterns of a conventional sonar. Programs were developed to cope with a variety of realistic geometrical configurations. Moreover, formulations were given for thick shells which included structure. All of these were based upon small signal theory.

The objective of the current program has been to extend our computational ability for the dome-transducer interaction to the nonlinear parametric case.

Simplifying assumptions are given along with their justification. We have utilized these assumptions to formulate a model in the idealistically simple case of an infinite planar dome-transducer interaction. From this model we can learn something about the sensitivity of parametric generation efficiency to variations in steering angle, dome thickness, and dome material properties. We can not learn anything about variation in radiation patterns from such a simple model. Nonetheless, by studying the planar case we feel that we have gained sufficient confidence to be able to recommend a procedure for computing the dome-transducer interaction for more realistic geometries drawing upon previously developed computer programs.

In the next two sections, the derivation[2] of our planar model will be presented. A subsequent section will give numerical results for both thick and thin planar domes showing the transmission loss.

## 2.0 PRIMARY FIELD SOLUTION[1]

The infinite planar dome-transducer model is shown in Fig. 1, along with the coordinate geometry. A thin plate is located a distance d from the planar "transducer". The transducer surface has a continuous normal velocity distribution which simulates the particle velocity of a plane wave traveling in a direction making an angle $\theta$ with the normal to the plane. This velocity distribution is given by

$$V = V_o e^{ik \times \sin\theta} \quad , \tag{1}$$

where $V_o$ is just a velocity amplitude factor. The pressure field between the dome and transducer will be denoted by $p_1$, and that outside the dome by $p_2$. In order for the fluid particle velocity to equal the transducer velocity at y = 0,

$$\frac{1}{i\omega\rho} \left.\frac{\partial p}{\partial y}\right|_{y=0} = V. \tag{2}$$

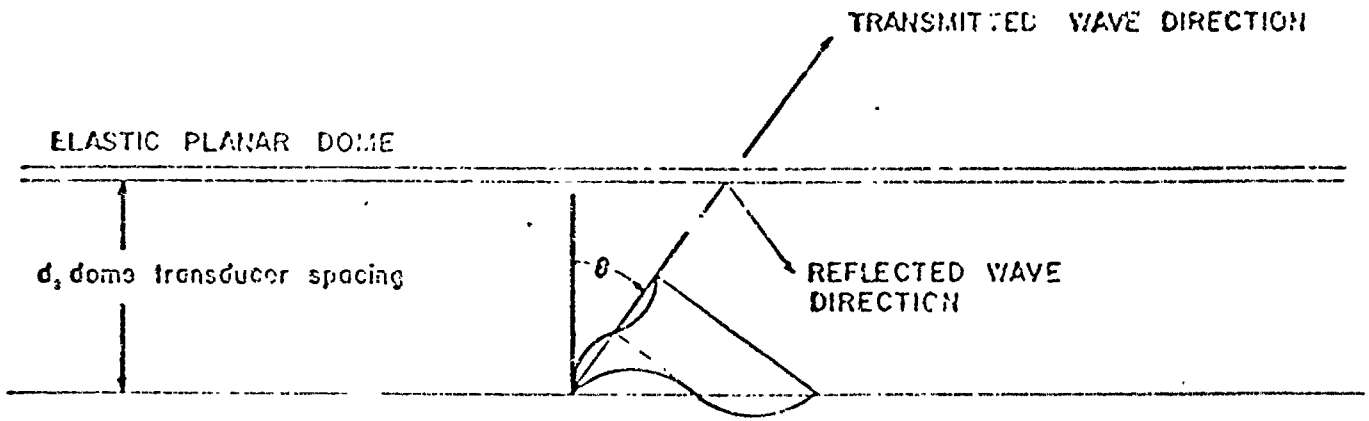


FIG. 1 - GEOMETRY OF INFINITE PLANAR DOME - TRANSDUCER MODEL

The plate is assumed to be thin enough so that the boundary conditions at its surfaces may be matched at the middle surface. One condition is that the fluid particle velocity at the inner and outer plate surfaces equal the plate velocity. If the plate displacement from equilibrium is denoted by u, the equality of velocities is given by

$$\frac{1}{i\omega\rho}\left[\frac{\partial p_1}{\partial y}\right]_{y=d} = \frac{1}{i\omega\rho}\left[\frac{\partial p_2}{\partial y}\right]_{y=d} = \frac{\partial u}{\partial t} . \tag{3}$$

The dynamic behavior of the plate is described by the classical plate equation. In this case, the driving force is the pressure difference across the plate, so that the equation of motion is

$$\left[p_1 - p_2\right]_{y=d} = \rho_s h \frac{\partial^2 u}{\partial t^2} + \frac{Eh^3}{12(1-\nu^2)} \frac{\partial^4 u}{\partial x^4} . \tag{4}$$

Here $\rho_s$ is the plate mass density, h is its thickness, E is Young's modulus, and $\nu$ is Poisson's ratio.

The solutions to the wave equation for the pressure fields inside and outside of the dome will have the forms

$$p_1 = \left[A\, e^{i\eta y} + B\, e^{-i\eta y}\right] e^{iKx} \quad , \quad \eta^2 + K^2 = k^2 \tag{5}$$

$$p_2 = C\, e^{i\eta y}\, e^{iKx} . \tag{6}$$

Substituting these equations into the boundary condition equations yields expressions for the unknown coefficients in Eqs. (4) and (5). The final results for the pressure fields are

$$p_1 = \frac{i\omega\rho\, V_o}{D}\left\{e^{i\eta(y-d)} + \frac{i\eta}{\omega^2\rho}(-\sigma\omega^2 + HK^4)\cos\eta(y-d)\right\}e^{iKx} \qquad (7)$$

$$p_2 = \frac{i\omega\rho\, V_o}{D}\, e^{i\eta(y-d)}\, e^{iKx} \,. \qquad (8)$$

where $\sigma = \rho_s h$ , $H = \frac{Eh^3}{12(1-\nu^2)}$ , $K = k \sin\theta$ , $\eta = k\cos\theta$

$$D = i\eta\left\{e^{-i\eta d} + \frac{\eta}{\omega^2\rho}(-\sigma\omega^2 + HK^4)\sin\eta d\right\} .$$

It is seen that $p_1$ is the sum of the traveling wave which is transmitted through the dome and a standing wave which always has an antinode at the plate. The average intensity passing through the plate is just

$$I_o = \frac{1}{2\rho c}\,\frac{(\omega\rho V_o)^2}{|D|^2} \,. \qquad (9)$$

For many cases of interest the $HK^4$ term in $D$ is small relative to $\sigma\omega^2$ . and we may write

$$D \approx i\eta\left\{e^{-i\eta d} - h\,\frac{\rho_s}{\rho}\,\eta\sin\eta d\right\}.$$

Defining T as the ratio of $I_o$ in Eq. (9) to the value that $I_o$ would have with no dome (i.e., h = 0), we have

$$T = 1/\left\{1 + \eta h \frac{\rho_s}{\rho} \sin \eta d \left[\eta h \frac{\rho_s}{\rho} \sin \eta d - 2 \cos \eta d\right]\right\}. \quad (10)$$

It is seen that T is a periodic function of d, with period $\pi/k \cos \theta$, and that its amplitude of oscillation decreases as $\theta$ increases. Starting from d = 0, T increases from unity until its first maximum occurs at a value of d for which

$$\tan 2 \eta d = 2/\eta h \, \rho_s/\rho \quad . \quad (11)$$

Typically, $\rho_s/\rho \approx 7.9$ and $kh \approx 1.7 \times 10^{-2}$, so that, for $\theta = 0$, Eq. (11) becomes approximately

$$\tan 2 \eta d = 14.1 \, .$$

This implies a plate-transducer spacing of .12 wavelengths. Maxima occur at this value of d and at every half wavelength thereafter.

To extend this solution to parametric excitation of the transducer, the velocity distribution is given by

$$V = V_o \left[ e^{ik_1 x \sin\theta} + e^{ik_2 x \sin\theta} \right] \quad . \quad (12)$$

Since the primary fields given in Eqs. (7) and (8) are obtained by solving the linear Helmholtz equation then superposition holds and we can immediately write down the solutions corresponding to Eq. (12). For example, in region 2 we shall have

$$P_{II} = i\rho V_o \left[ \frac{\omega_1}{D_1} e^{i\eta_1 (y-d)} e^{iK_1 x} + \frac{\omega_2}{D_2} e^{i\eta_2 (y-d)} e^{iK_2 x} \right]. \quad (13)$$

## 3.0 SECONDARY FIELD SOLUTION

The secondary radiation field $P_-$ is given by the linearized Helmholtz equation

$$\left(\nabla^2 + k_-^2\right) \hat{P}_- = + \frac{k_-^2 \beta \hat{P}_2 \hat{P}_2^*}{\rho c_o^2} . \quad (14)$$

$\beta \doteq 3.8$ for sea water; $\hat{P}_2$, $\hat{P}_2^*$ are the time independent primary field solutions outside the dome at the two primary frequencies. The solution of Eq. (14) is given by

$$\hat{P}_{2-} = \frac{k_-^2 \beta}{\rho c_o^2} \int_h^{\infty} \int_{-\infty}^{+\infty} r_2 \hat{P}_2 \hat{P}_2^* \, dx \, dy . \quad (15)$$

In practice, the $\infty$ limit on y can be replaced by a finite limiting distance when $\hat{P}_2 \hat{P}_2^*$ becomes much less than unity. Inside the dome the solution is

$$\hat{P}_{1-} = \frac{k_-^2 \beta}{\rho c_o^2} \int_0^d \int_{-\infty}^{+\infty} \Gamma_1 \hat{P}_1 \hat{P}_1^* \, dx \, dy \quad . \tag{16}$$

$\hat{P}_1$, $\hat{P}_1^*$ are the time independent primary field solutions inside the dome. Now $\Gamma_1$ and $\Gamma_2$ are the Green's functions for inside and outside the dome respectively.

An appropriate Green's function[2] for region 1 inside the dome is given by the method of images as

$$G\left(\vec{r} \mid \vec{r}_o\right) = \pi i \sum_{n=-\infty}^{+\infty} \left[ H_o^{(1)}\left(k_- \left| \vec{r} - \vec{r}_\eta' \right|\right) - H_o^{(1)}\left(k_- \left| \vec{r} - \vec{r}_\eta'' \right|\right)\right] \tag{17}$$

where $$r_\eta' = a_y \left[2nd + y_o\right] + a_x x_o$$

$$r_\eta = a_y \left[2nd - y_o\right] + a_x x_o \quad .$$

In region 1 inside the dome, the boundary conditions on $\Gamma_1$ are:

$$\Gamma_1 = 0 \text{ at } y = 0 \text{ (transducer)}$$

and $$\Gamma_1 = g \text{ at } y = d$$

where g in most cases will be much less than unity.

In region 2 outside the dome $\Gamma_2$ must also satisfy the condition $\Gamma_2 = g$. For many applications the dome-transducer spacing will only be a few wavelengths of the primary beams. To a good approximation no secondary field has been generated at the dome. Therefore, the boundary condition at the dome becomes $\Gamma_2 = 0$.

An appropriate Green's function[2] for region 2 is

$$\Gamma_2\left(r \mid r_o\right) = \pi i \left[H_o^{(1)}\left(k\_R\right) - H_o^{(1)}\left(k\_R_o\right)\right] \quad . \quad (18)$$

Fig. 2 shows R and $R_o$ for a source point outside the dome. The structure of Eqs. (17) and (18) already guarantees that $\Gamma_2$ vanishes at $r = \infty$ and that both $\Gamma_1$ and $\Gamma_2$ are singular at $r = r_o$ .

Without greatly complicating Eqs. (15) and (16), we can allow either for small signal attenuation or finite amplitude saturation effects.

The following parameters can be varied:

1. primary frequencies
2. dome elastic properties
3. dome-transducer spacing
4. angle of incidence of beams on dome

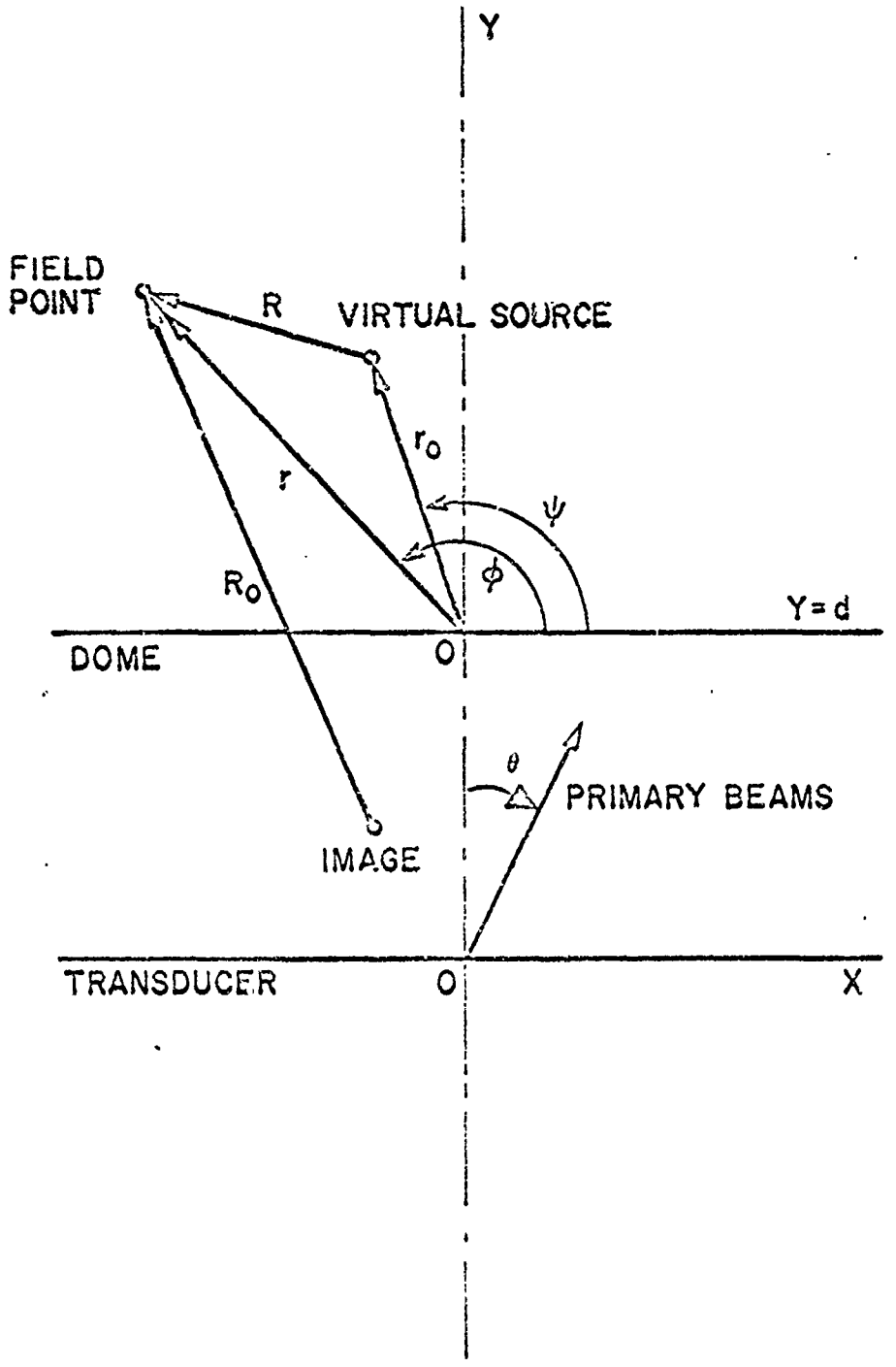


FIG. 2 GEOMETRY PERTINENT TO $\Gamma_2$ AND THE CALCULATION OF $P_2(\omega_-)$.

If it is desirable, the active portion of the plane transducer can be limited along the x coordinate. This is accomplished by replacing the continuous normal velocity distribution of Eq. (1) by

$$\begin{aligned} V &= V_o e^{ikx \sin\theta} && |x| \leq a \\ &= 0 && |x| > a \ . \end{aligned} \tag{19}$$

The velocity distribution V given by Eq. (19) can be represented by a spatial fourier series in an approximate fashion.

## 4.0 THE INTEGRAL FOR $\hat{P}_2(\omega_-)$

If we ignore any generation of $P_1(\omega_-)$ in region 1 then $\Gamma_2$ satisfies the boundary condition $\Gamma_2 = 0$ at the dome surface. As shown in Fig. 2 it is perfectly consistent with this assumption to consider our origin of coordinates on the dome surface. With reference to Fig. 2, we see that

$$R^2 = r_o^2 + r^2 - 2r_o r \cos(\phi - \psi) \tag{20}$$

and

$$R_o^2 = r_o^2 + r^2 + 2r_o r \cos(\phi - \psi) \ . \tag{21}$$

For the infinite planar geometry of our problem, it is not correct to distinguish between near and far fields. The virtual parametric array is theoretically a tapered end fire array that is infinitely long ( $r_o \longrightarrow \infty$ ). Practically speaking, it has significant source strength for a finite distance. For our purposes, it will be permissible to truncate this array at $r_o^* = \frac{1}{\alpha_1 + \alpha_2}$ where $\alpha_1$ and $\alpha_2$ are the

small signal attenuation coefficients of the primary beams. If we take our field point r to be ten times larger than the maximum value for $r_o$, i.e., $r_o^*$, then Eqs. (20) and (21) can be simplified and take the form

$$R \doteq r - r_o \cos(\phi - \psi) \tag{22}$$

and

$$R_o \doteq r + r_o \cos(\phi - \psi) . \tag{23}$$

Moreover, we can choose r large enough, so that $k_- r >> 1$. Then the large argument assymptotic formula for the Hankel function can be used to simplify $\Gamma_2$. Thus $\Gamma_2$ becomes

$$\Gamma_2 = i\sqrt{\frac{2\pi}{k_-}}\, e^{-i\pi/4}\left[\frac{e^{ik_-R}}{\sqrt{R}} - \frac{e^{ik_-R_o}}{\sqrt{R_o}}\right] \tag{24}$$

If we substitute Eq. (24) into Eq. (15) and change to polar coordinates we obtain

$$\frac{\hat{P}_2}{P_o} = A\int_o^{\pi}\int_o^{r_o^*}\left(\frac{e^{ik_-R}}{\sqrt{R}} - \frac{e^{ik_-R_o}}{\sqrt{R_o}}\right) e^{-(a_1+a_2)z} \cdot e^{-ik_- r_o \sin(\psi+\theta)}\, r_o\, dr_o\, d\psi . \tag{25}$$

Here A is given by

$$A = \frac{\beta P_0 k_-^{3/2} \omega_1 \omega_2 \sqrt{2\pi}\, e^{i\left(\frac{\pi}{4} + dk_- \cos\theta\right)}}{\rho_c c_0^4 D_1 L_2^*} \qquad (26)$$

and z represents the attenuation path length of the primary beams to the source point as shown in Fig. 2.

$$z = \frac{r_o \sin\psi}{\cos\theta} \qquad (27)$$

Eq. (25) allows us to calculate the amplitude of the difference frequency field at any point $(r, \phi)$. It is to be noted that the physical parameters relating to the thin dome enter only into the coefficient A via $D_1$ and $D_2^*$. In the thick dome case, this coefficient will also contain the dome parameters. By letting the dome thickness $h \longrightarrow 0$, we can find the limiting value for A in the absence of a dome. If we are only interested in the relative change in amplitude of $P_-$ at a field point $(r, \phi)$, then it is only necessary to compute the following ratio

$$\frac{A \text{ (with dome thick or thin model)}}{\lim_{h \longrightarrow 0} A \text{ (thin)}} \qquad (28)$$

The integral in Eq. (25) is the same for both numerator and denominator of Eq. (28) and can be cancelled.

The expression for A in the thick dome case was derived with results given by Brekhovskikh[3]. A detailed derivation was presented in the Third Quarterly Report and will not be repeated here.

Before presenting numerical results, we should like to list the key assumptions of our planar dome model:

1. In practice, the dome-transducer spacing will only be of the order of 10 primary wavelengths. Therefore all parametric generation both within the dome itself and between the dome and transducer can be ignored.

2. Small signal theory is used to compute the transmitted amplitudes of the primary beams.

3. In a finite amplitude radiation field, the finite pressure gradients can give rise to hydrodynamic flow termed streaming. Owing to the proximity of the dome inner surface it is felt that it is unlikely that pressure gradients which are large enough to produce streaming will occur. Moreover, pulsed source operation seems to prevent streaming.

4. We assume that most of the energy is transmitted through the dome. Eqs. (10) and (11) indicate that there are periodic maxima in the transmission coefficient as d is varied. As will be seen in the next section, some standing wave resonance effects will occur for particular values of d. However even for these cases most of the acoustical energy is transmitted through the dome; hence, it is felt that assumptions 1 and 2 will still be valid.

## 5.0 NUMERICAL RESULTS

In an effort to gain some insight into the dependence of parametric array transmitted power on dome-transducer interactions, the simple model of an infinite planar transducer and planar dome was analyzed. While the infinite planar dome-transducer model cannot be used to predict beam patterns and source levels, it clearly displays the dependence of transmitted power on both steering angle and dome-transducer spacing. Further, the mathematical form of the pressure field solution for the primary frequencies can be readily analyzed to separate the standing wave between dome-transducer and the wave transmitted through the dome.

In our model, the "transducer" was an infinite plane with a continuous normal velocity distribution which simulated the particle velocity of a plane wave steered in a direction making an angle $\theta$ with the normal to the plane. The wave outside the dome was just such a plane wave; however, the dome modified its amplitude and phase. Inside the dome-transducer cavity, the pressure field consisted of a plane wave traveling in the outward direction and a reflected wave traveling in the inward direction. These two waves included the direct transmission and all of the multiply-reflected components. The sum of all these components add to yield a net transmitted wave plus a standing wave.

The dome was modeled as either a lossless elastic plate[1] or a lossless elastic medium[3]. These two dome models are referred to as "thin" and "thick", respectively. It should be noted that the thin model did not admit waves internal to the dome while the thick model did.

For both models the time average intensity transmitted through the plate was periodic with $k_p d\cos\theta$, where $k_p$ was one of the primary frequency wave numbers, d was the dome-transducer spacing, and $\theta$ was the steering angle. This periodicity with $k_p d\cos\theta$, coupled with the fact that the models are lossless and the plates infinite in extent, means that resonances will exhibit themselves with respect to both the dome-transducer cavity and, for the thick model, the dome itself.* These effects can result in parameter combinations where the intensity with dome, normalized to the no-dome intensity, exceeds one. A discussion of this for the linear, single frequency case can be found in Section 2.0.

Representative results of this analysis are presented in Figs. 3 through 14. The parameters used in this study are given in Table I. No special significance should be attached to the parameters selected except that they seemed "reasonable" to assess the effects of the two dome models on the acoustic interaction. One moderating factor was that the only measured data we were aware of was a measurement made by Konrad, NUSC/NL, involving a steel plate.** That comparison is shown in Fig. 15 and will be discussed in detail later.

---

*The significance of resonance is that we are changing the impedance the transducer sees. Because we assumed a velocity control situation, we therefore change the power out of the transducer as a function of dome-transducer spacing and dome thickness.

**These results were communicated privately to Dr. Cary by Mr. Konrad.

TABLE I

SUMMARY, MODEL PARAMETERS

| | |
|---|---|
| Primary Frequencies | 50 kHz<br>60 kHz |
| Dome Material | Steel |
| h | 0.0 - 1.2 inches |
| $\rho_s$ | $7.35(10)^{-4}$ $\frac{lb_f\text{-sec}^2}{in.^4}$ |
| E | $30(10)^6$ $lb_f/in.^2$ |
| $\nu$ | 0.3 |
| $C_L$ | $2.34(10)^5$ in./sec |
| $C_S$ | $1.25(10)^5$ in./sec |
| Fluid | Water |
| c | 60,000 in./sec |
| $\rho$ | $9.66(10)^{-5}$ $\frac{lb_f\text{-sec}^2}{in.^4}$ |
| Dome-Transducer Spacing | 9.25 - 10.5 in. |
| Steering Angles | 0°, 20° |

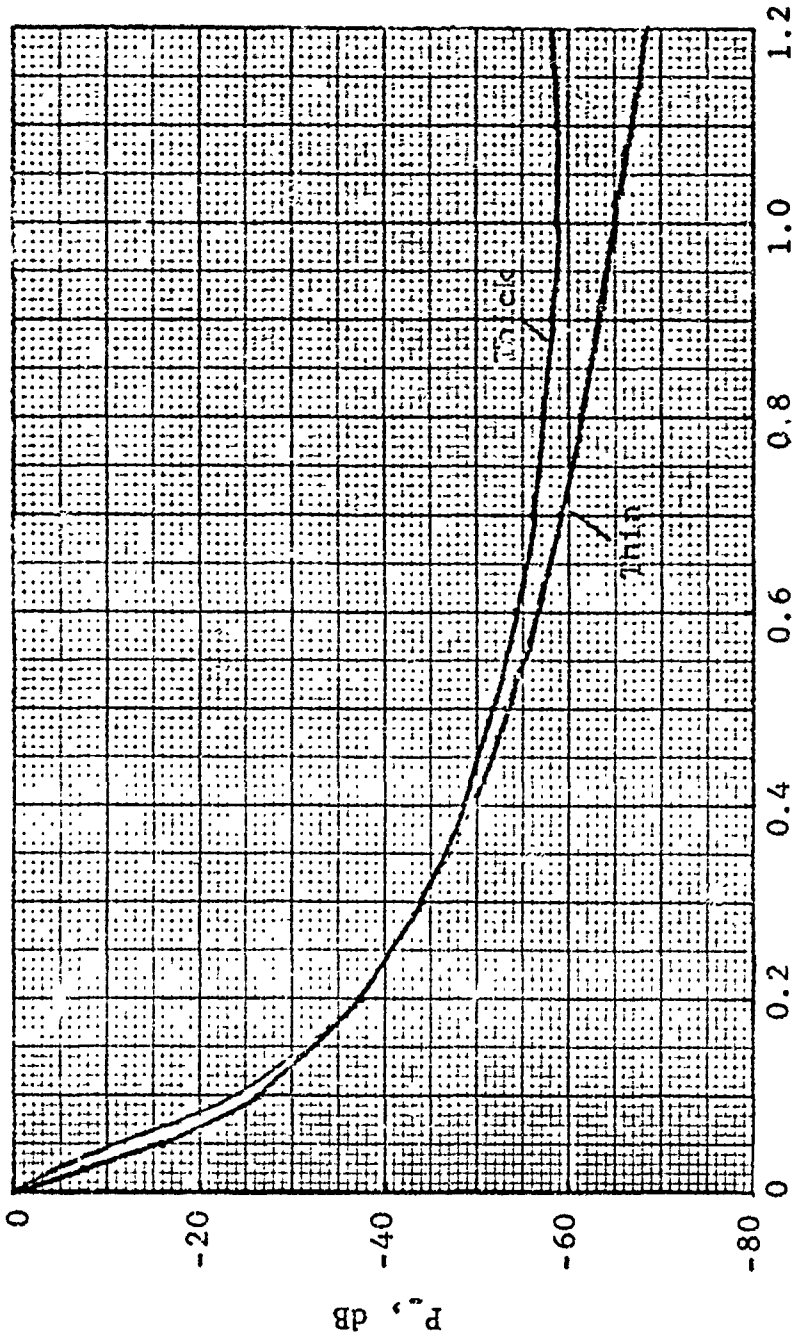


FIG. 3 - NORMALIZED FARFIELD DIFFERENCE FREQUENCY PRESSURE VS. DOME THICKNESS, SPACING 9.25 in., STEERING 0°

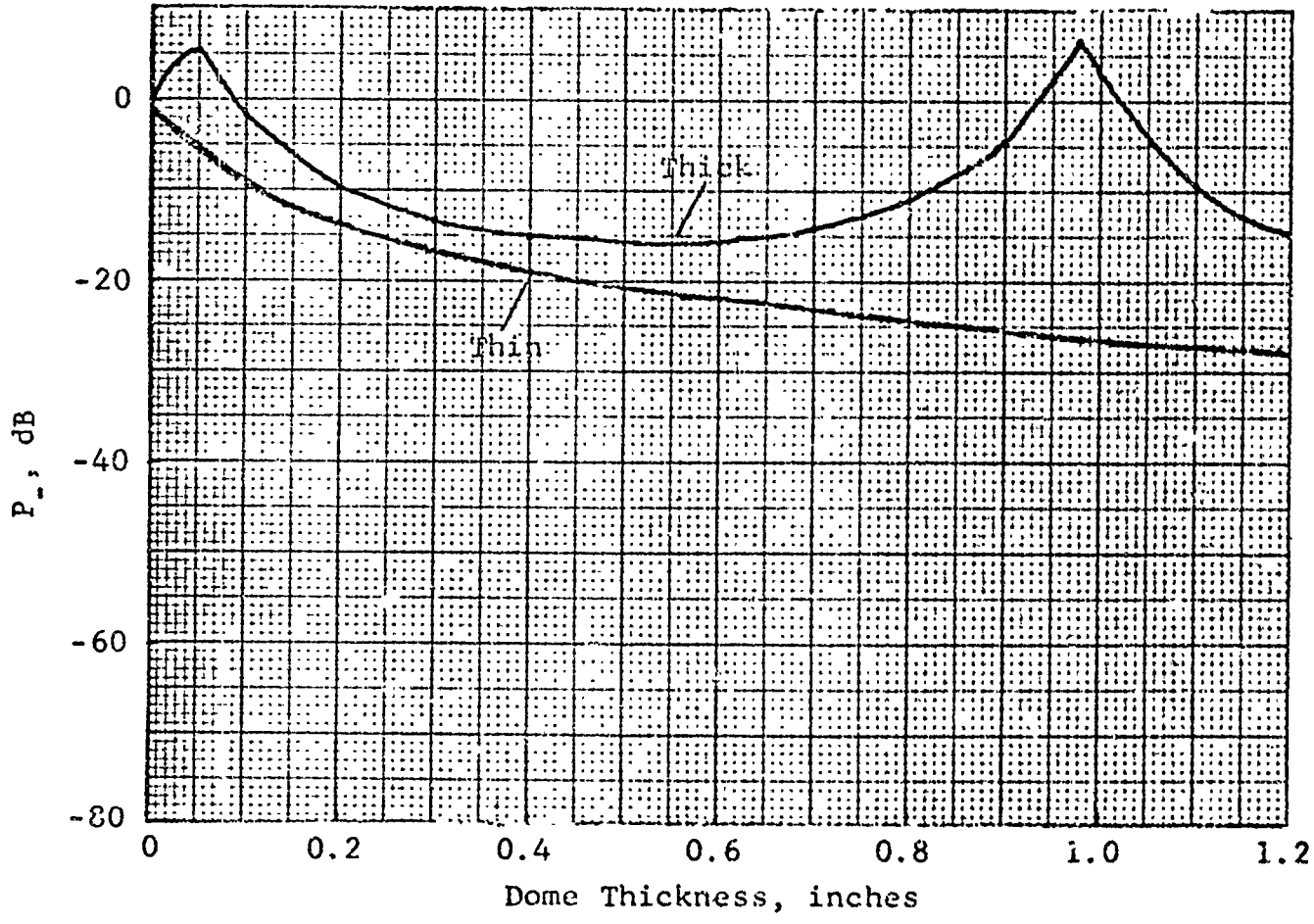


FIG. 4 - NORMALIZED FARFIELD DIFFERENCE FREQUENCY PRESSURE VS. DOME THICKNESS, SPACING 9.5 in., STEERING 0°

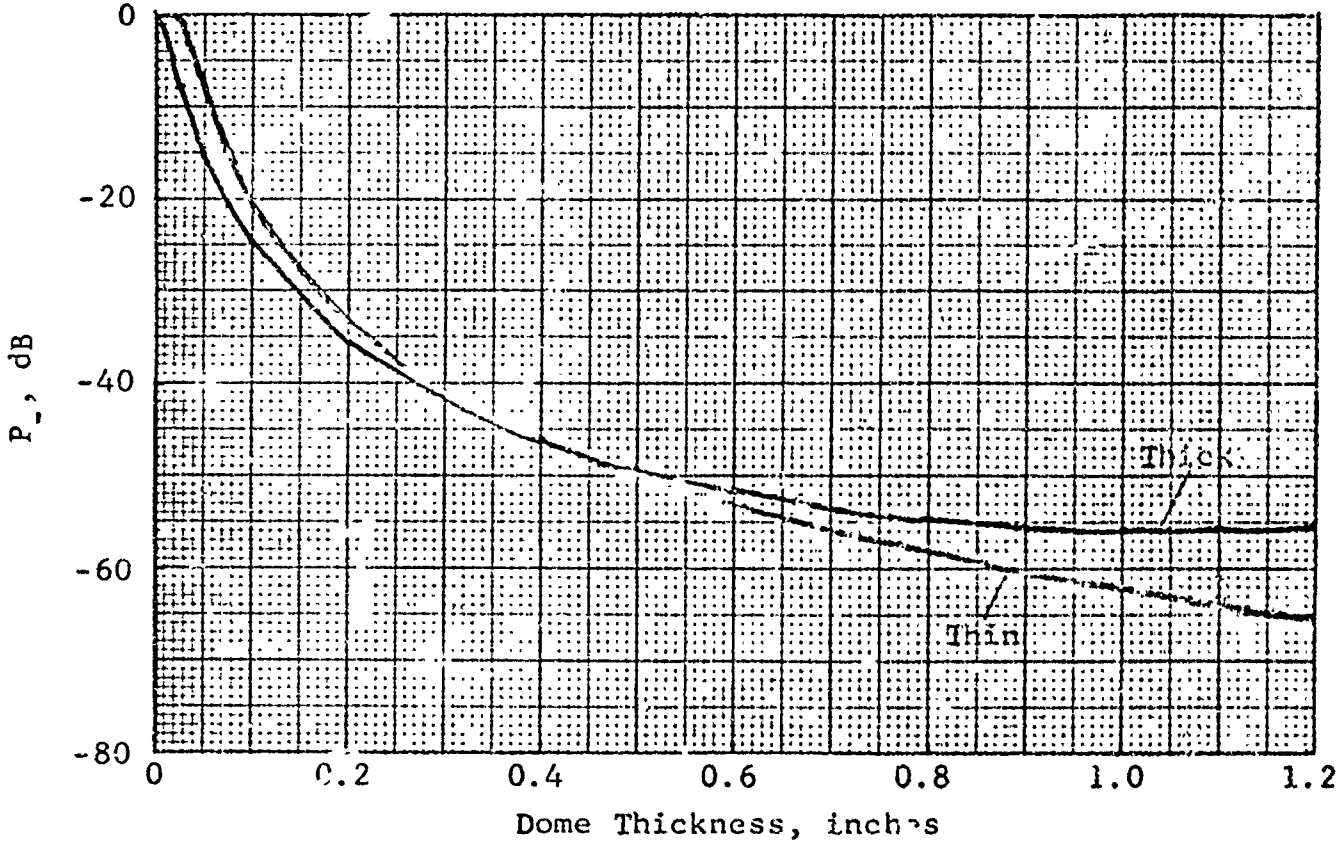


FIG. 5 - NORMALIZED FARFIELD DIFFERENCE FREQUENCY PRESSURE VS. DOME THICKNESS, SPACING 9.75 in., STEERING 0°

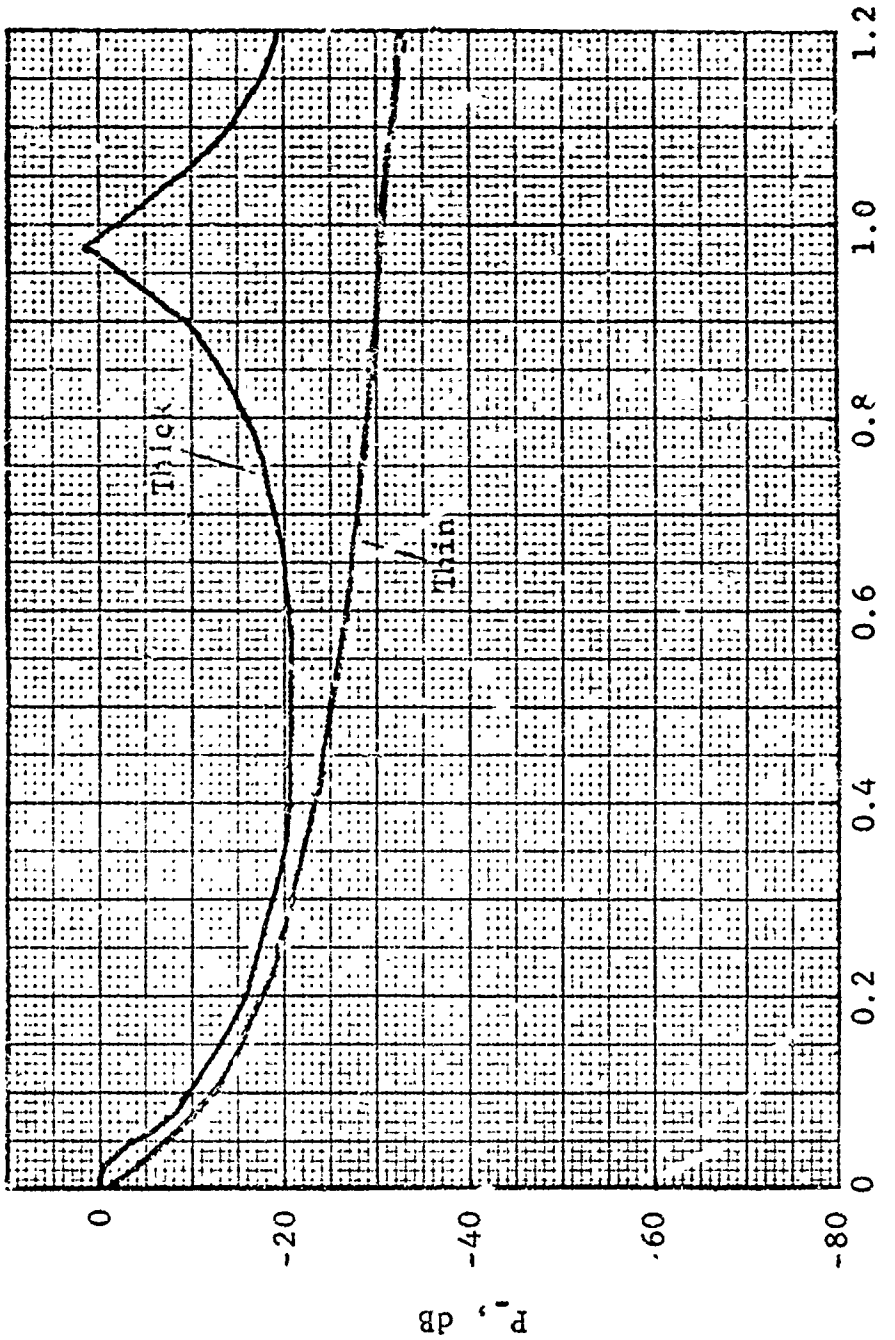


FIG. 6 - NORMALIZED FARFIELD DIFFERENCE FREQUENCY PRESSURE VS. DOME THICKNESS, SPACING 10.0 in., STEERING 0°

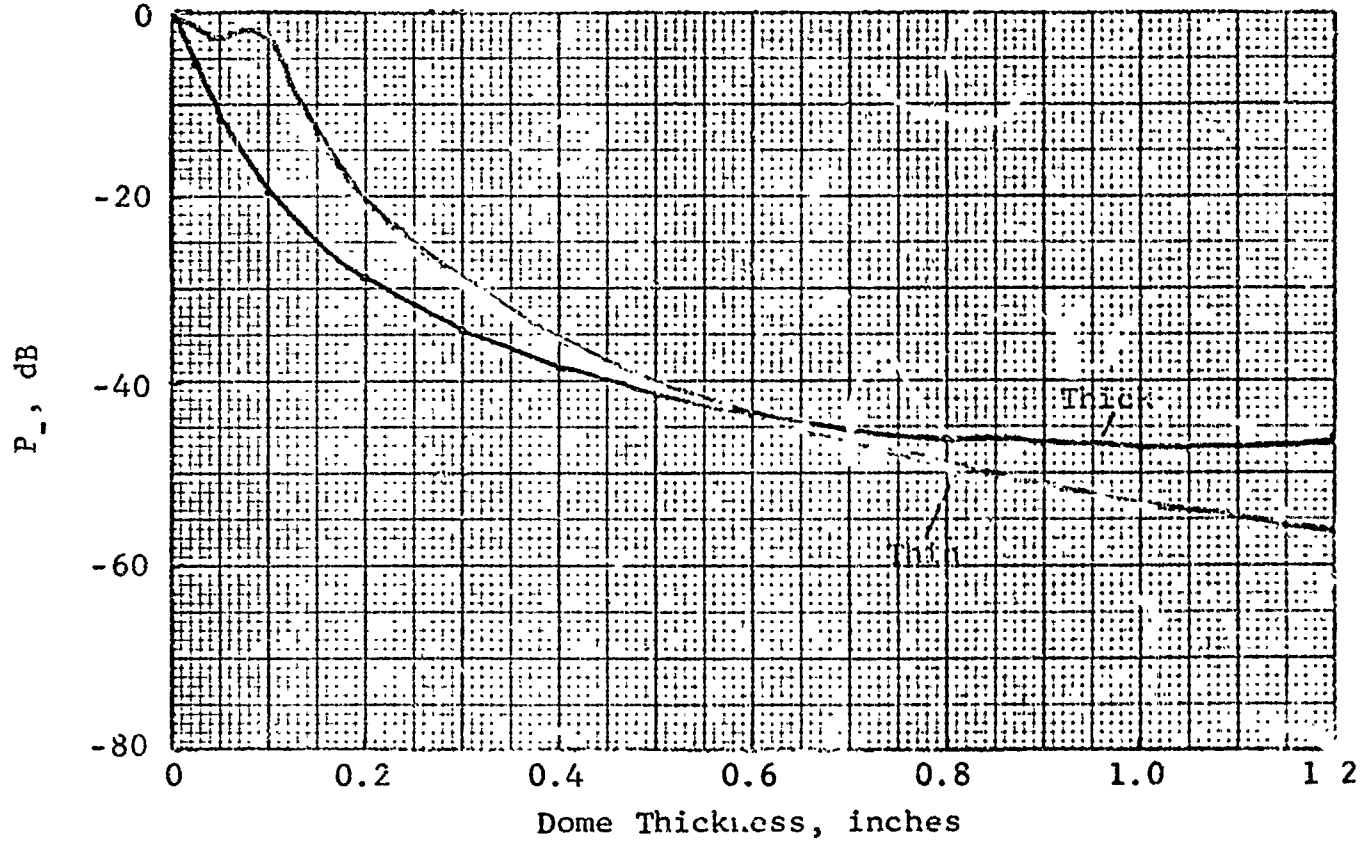


FIG. 7 - NORMALIZED FARFIELD DIFFERENCE FREQUENCY PRESSURE VS. DOME THICKNESS, SPACING 10.25 in., STEERING 0°

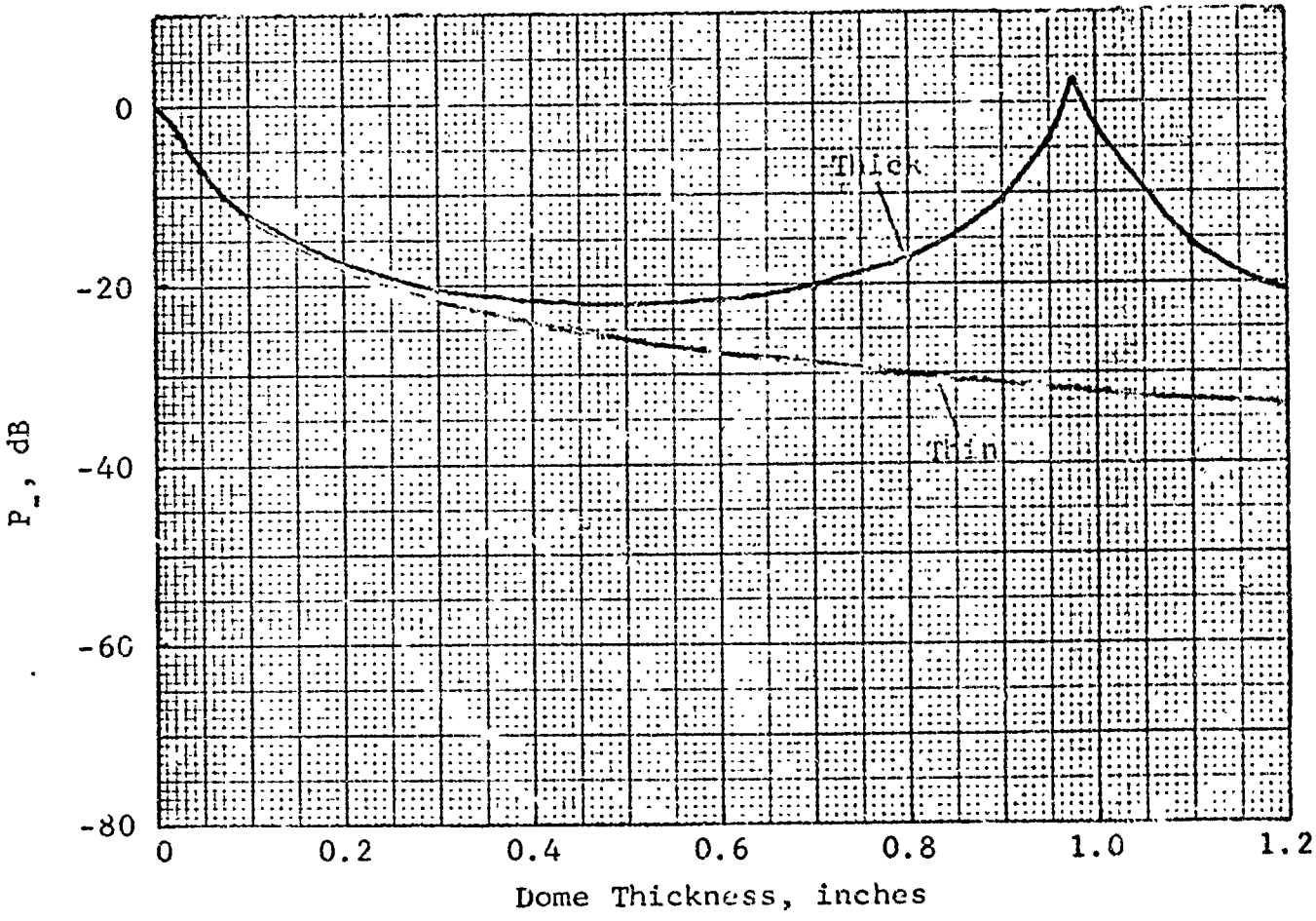


FIG. 8 - NORMALIZED FARFIELD DIFFERENCE FREQUENCY PRESSURE VS. DOME THICKNESS, SPACING 10.5 in., STEERING 0°

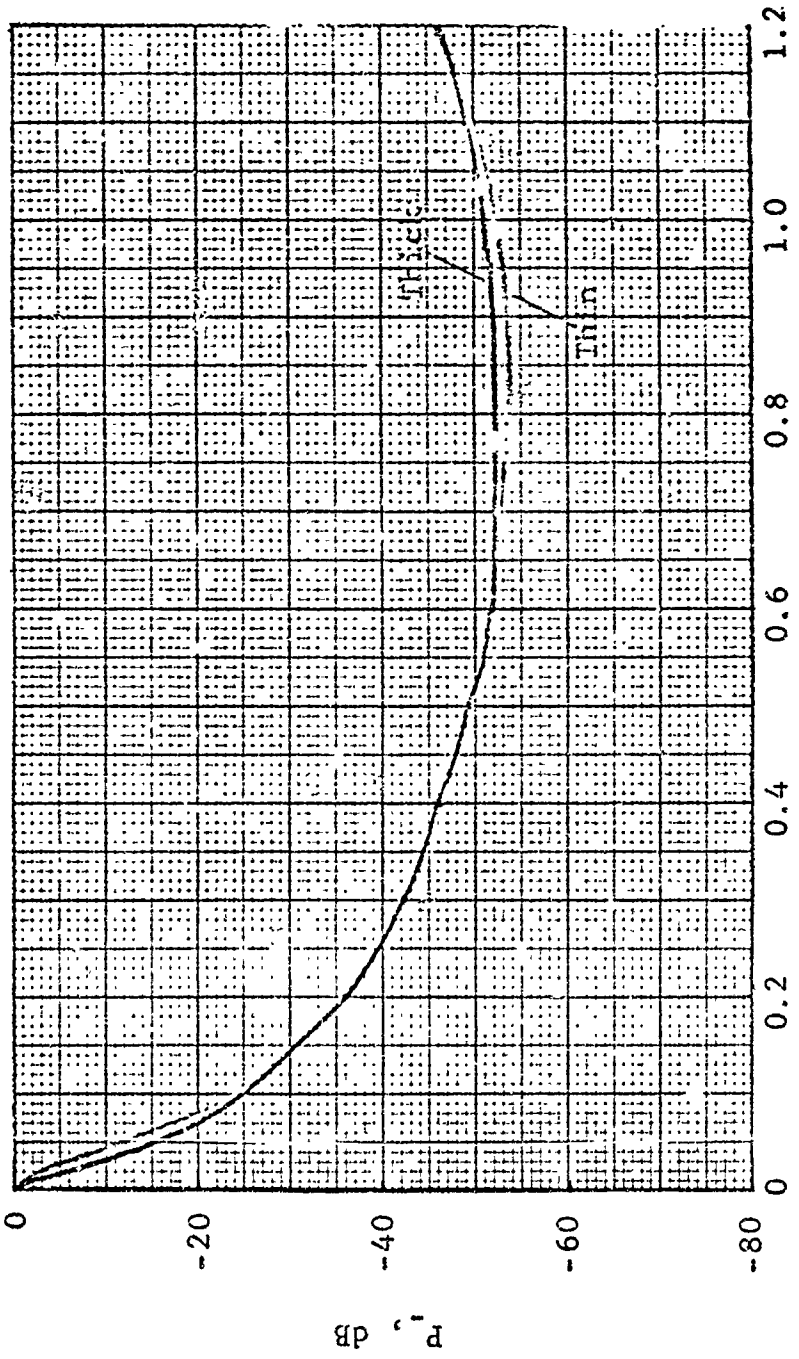


FIG. 9 - NORMALIZED FARFIELD DIFFERENCE FREQUENCY PRESSURE VS. DOME THICKNESS, SPACING 9.25 in., STEERING 20°

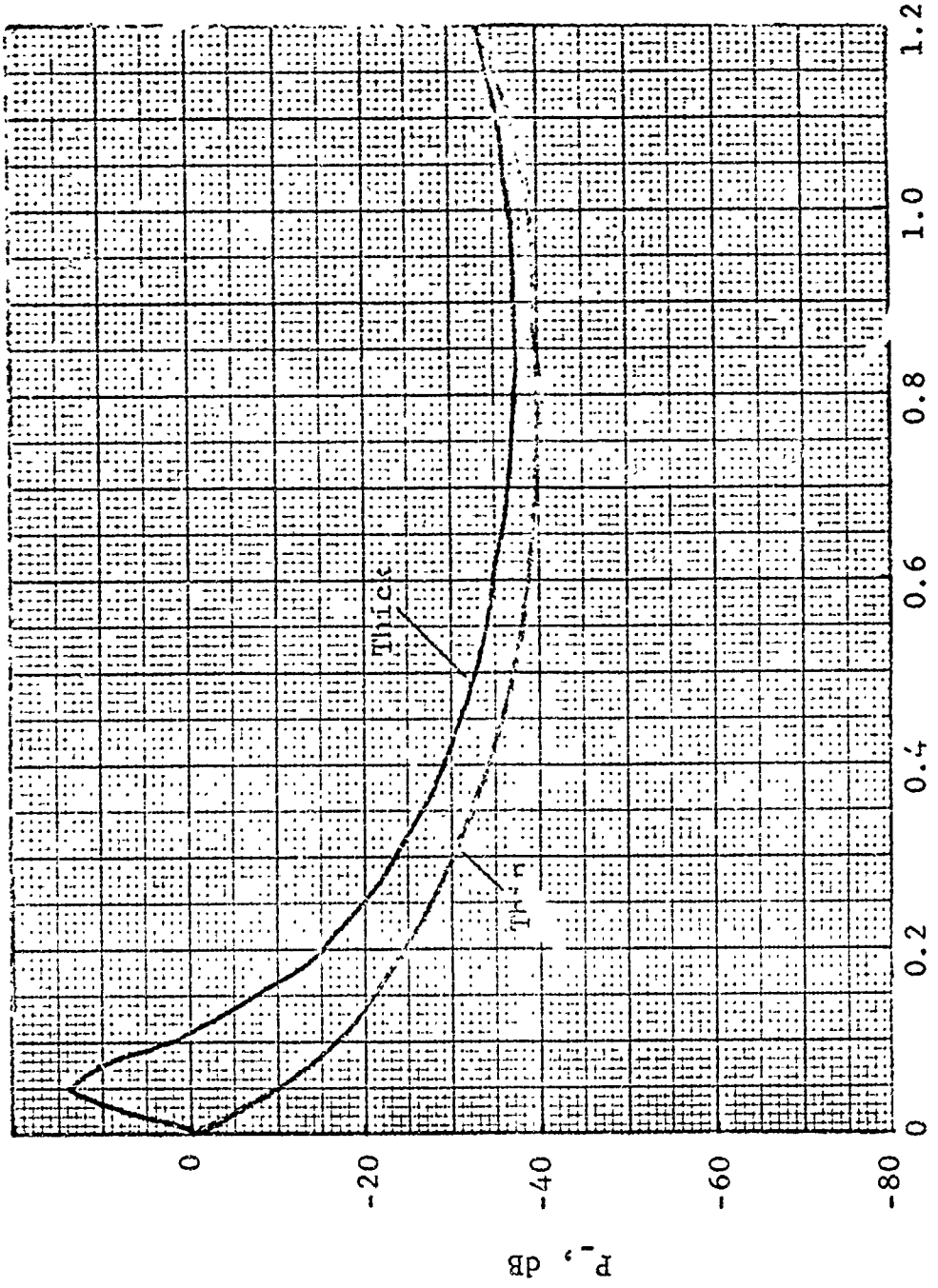


FIG. 10 - NORMALIZED FARFIELD DIFFERENCE FREQUENCY PRESSURE VS. DOME THICKNESS, SPACING 9.5 in., STEERING 20°

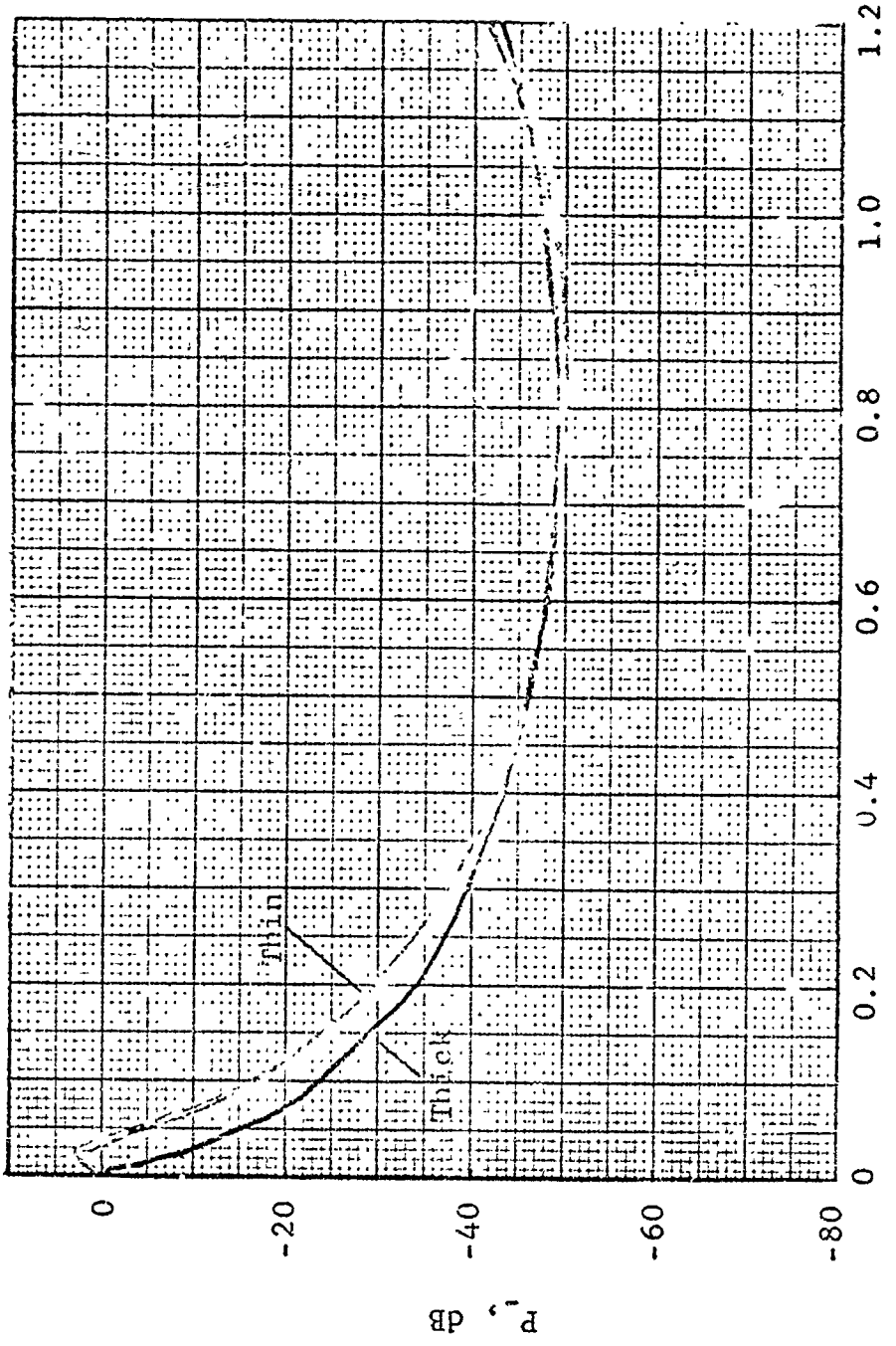


FIG. 11 - NORMALIZED FARFIELD DIFFERENCE FREQUENCY PRESSURE VS. DOME THICKNESS, SPACING 9.75 in., STEERING 20°

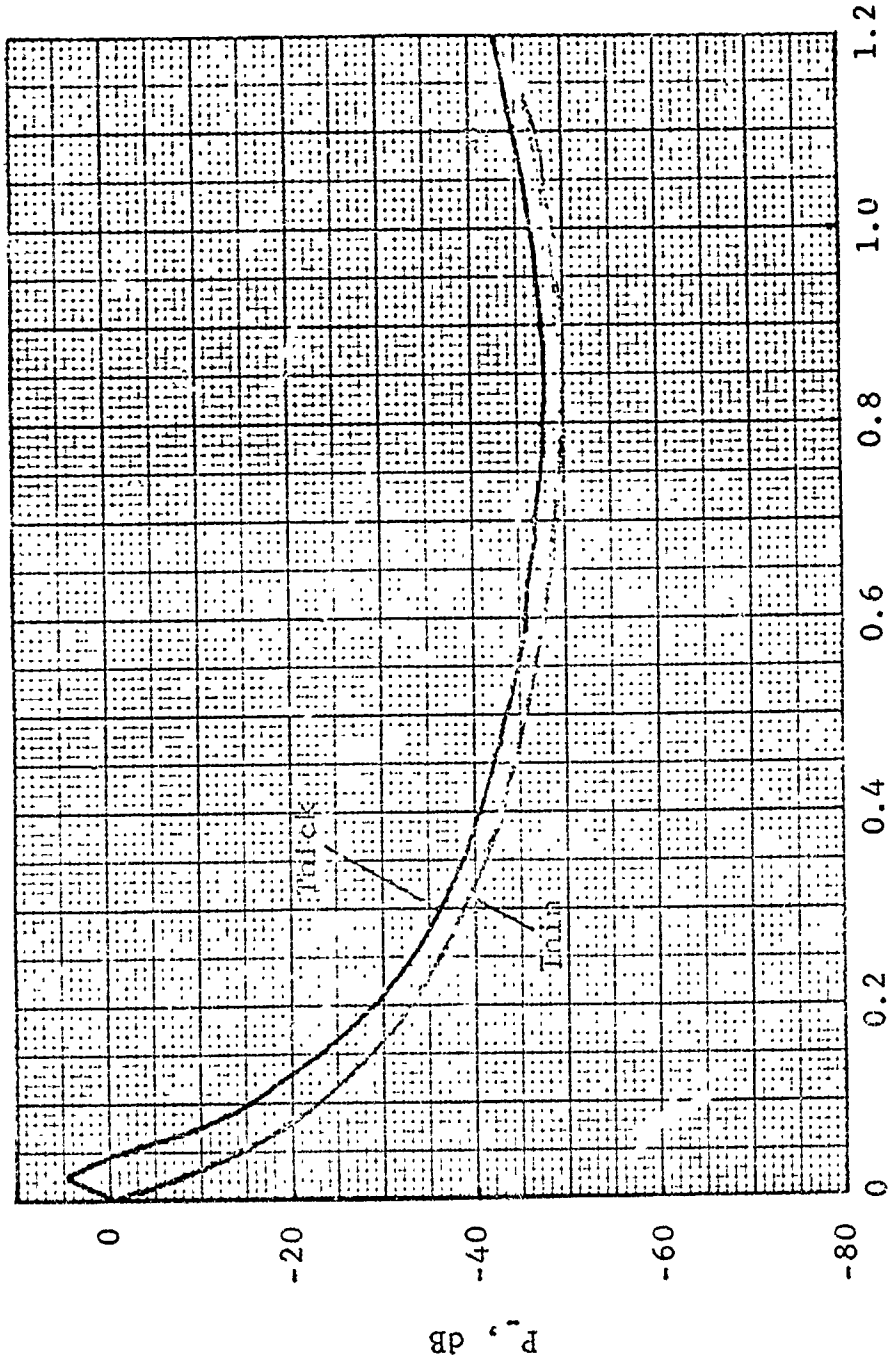


FIG. 12 - NORMALIZED FARFIELD DIFFERENCE FREQUENCY PRESSURE VS. DOME THICKNESS, SPACING 10.0 in., STEERING 20°

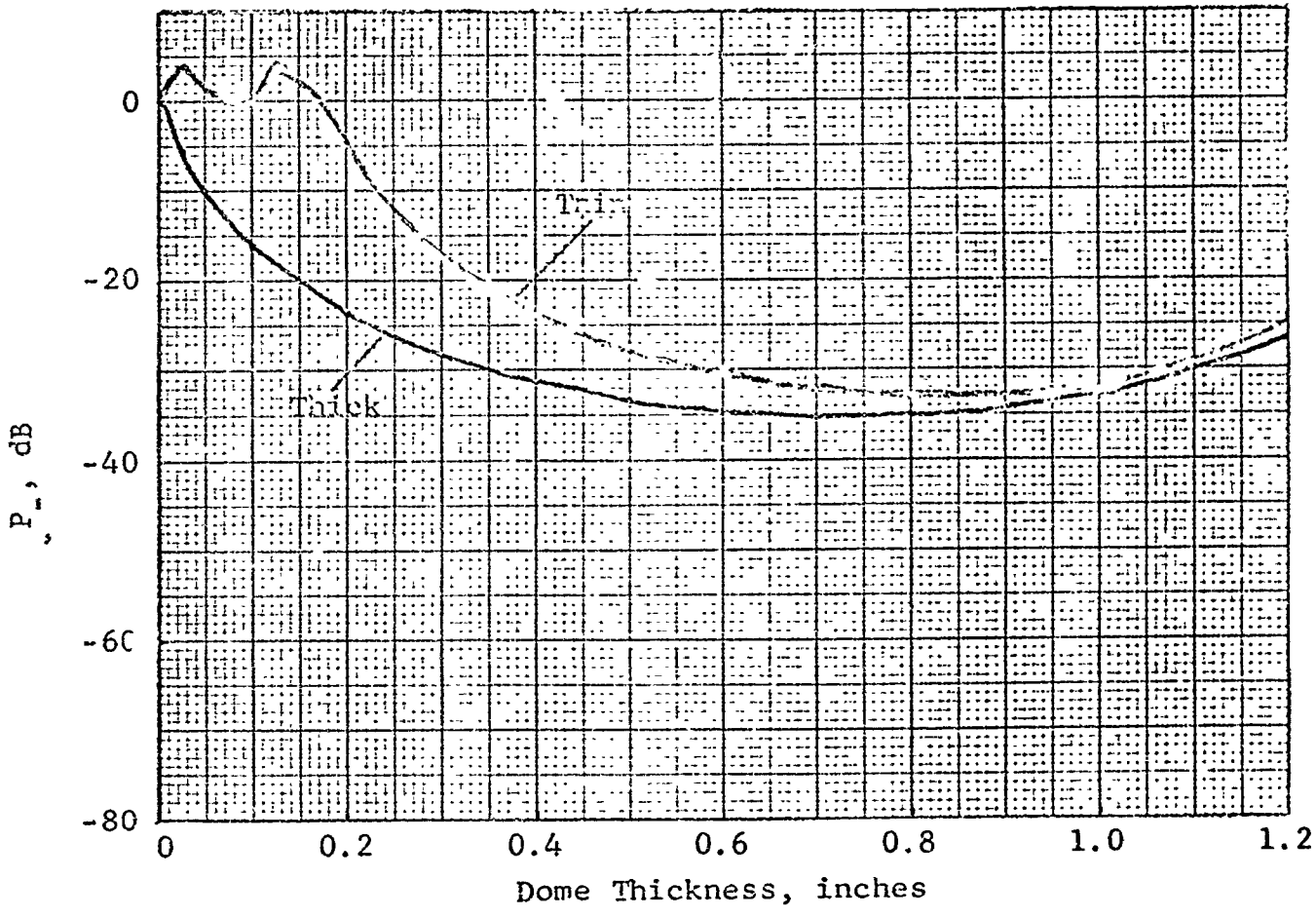


FIG. 13 - NORMALIZED FARFIELD DIFFERENCE FREQUENCY PRESSURE VS. DOME THICKNESS, SPACING 10.25 in., STEERING 20°

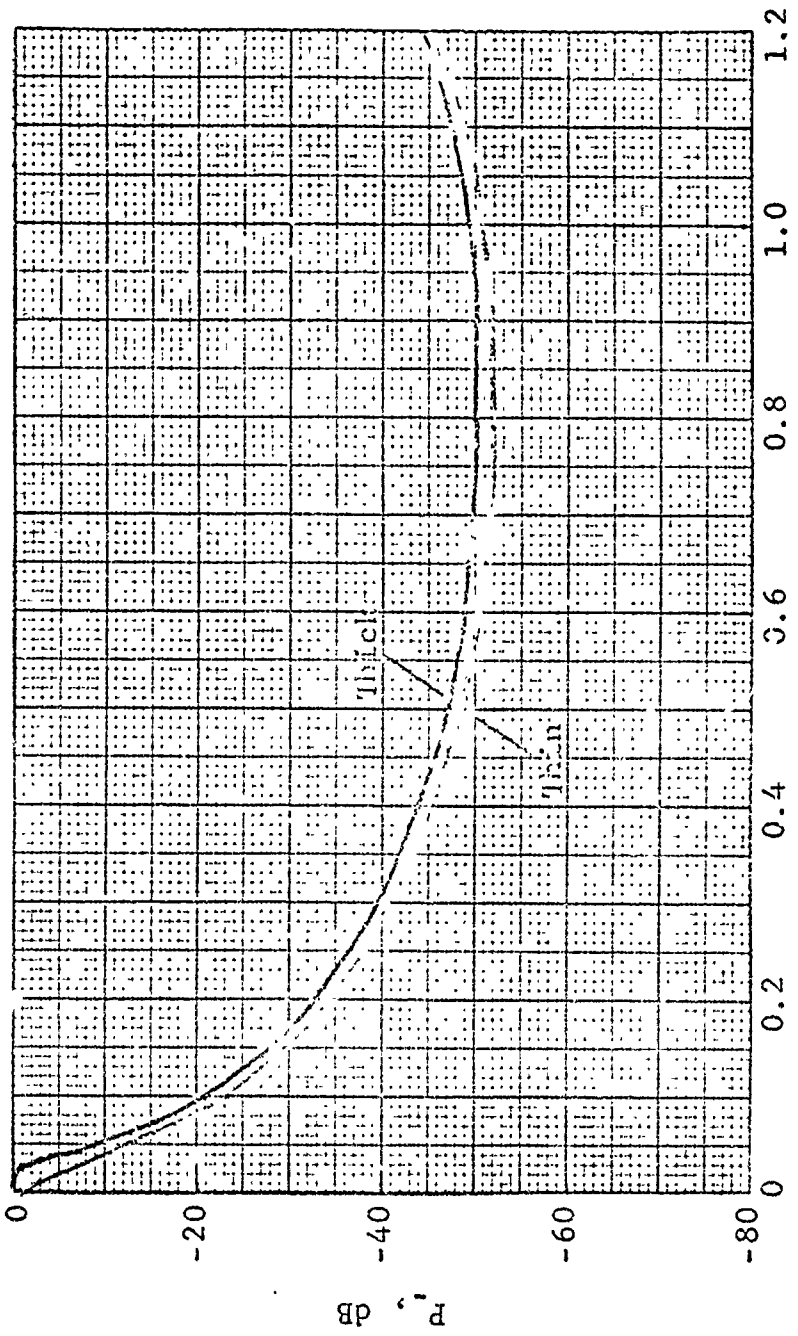


FIG. 14 - NORMALIZED FARFIELD DIFFERENCE FREQUENCY PRESSURE VS. DOME THICKNESS, SPACING 10.5 in., STEERING 20°

In each of Figs. 3 through 14, the ordinate is the difference frequency pressure with dome, normalized to the difference frequency pressure without dome. The abscissa is the dome thickness in inches. Each figure shows the results obtained for both the thick and thin models. In Figs. 3 through 8, the results for $0^\circ$ steering are presented. The periodicity of the results with $k_p d\cos\theta$ is very evident in these results. For example, Fig. 3 shows good agreement between thick and thin; furthermore, this separation does not correspond to a multiple wavelength spacing at either primary frequency in the dome-transducer cavity; therefore, any standing wave effects are minimized. On the other hand, in Fig. 4 we see poorer agreement and significantly less transmission loss than in Fig. 3. For the results shown in Fig. 4 we have selected a dome-transducer spacing resulting in a resonance condition at 60 kHz. This effect is, of course, amplified by the ideal geometry and lack of damping in our model.

The thick model resonance out around 1.0 inch is due to a quarter wavelength thickness of the dome at one of the primary frequencies. Notice that this internal dome resonance does not occur in Fig. 3 where we do not have a strong standing wave pattern built up in the dome-transducer cavity. The upturn of the thick result in Fig. 3 is caused by the onset of a half wavelength resonance in the material which occurs at a thickness of approximately 2 inches. It should also be realized that the resonance seen in Fig. 4 in the thick model is very sensitive to dome-transducer spacing and that a slightly different spacing would result in the disappearance of the peak at about 1 inch and merge the two results as in Fig. 3.

## TABLE II

## PARAMETERS, MEASURED DATA

| | |
|---|---|
| Primary Frequencies (measured) | 246 kHz<br>234 kHz |
| Dome Material | Steel |
| h (measured) | 0.087 in. |
| $\rho_s$ (assumed) | $7.35(10)^{-4}$ $\frac{lb_f\text{-}sec^2}{in.^4}$ |
| E (assumed) | $30(10)^6$ $lb_f/in.^2$ |
| $\nu$ (assumed) | 0.3 |
| $C_L$ (assumed) | $2.34(10)^5$ in./sec |
| $C_S$ (assumed) | $1.25(10)^5$ in./sec |
| Fluid | Water |
| c (assumed) | 60,000 in./sec |
| $\rho$ (assumed) | $9.66(10)^{-5}$ $\frac{lb_f\text{-}sec^2}{in.^4}$ |
| Dome-Transducer Spacing (measured) | 3.0 in. |
| Steering Angle (measured) | 10.0° |

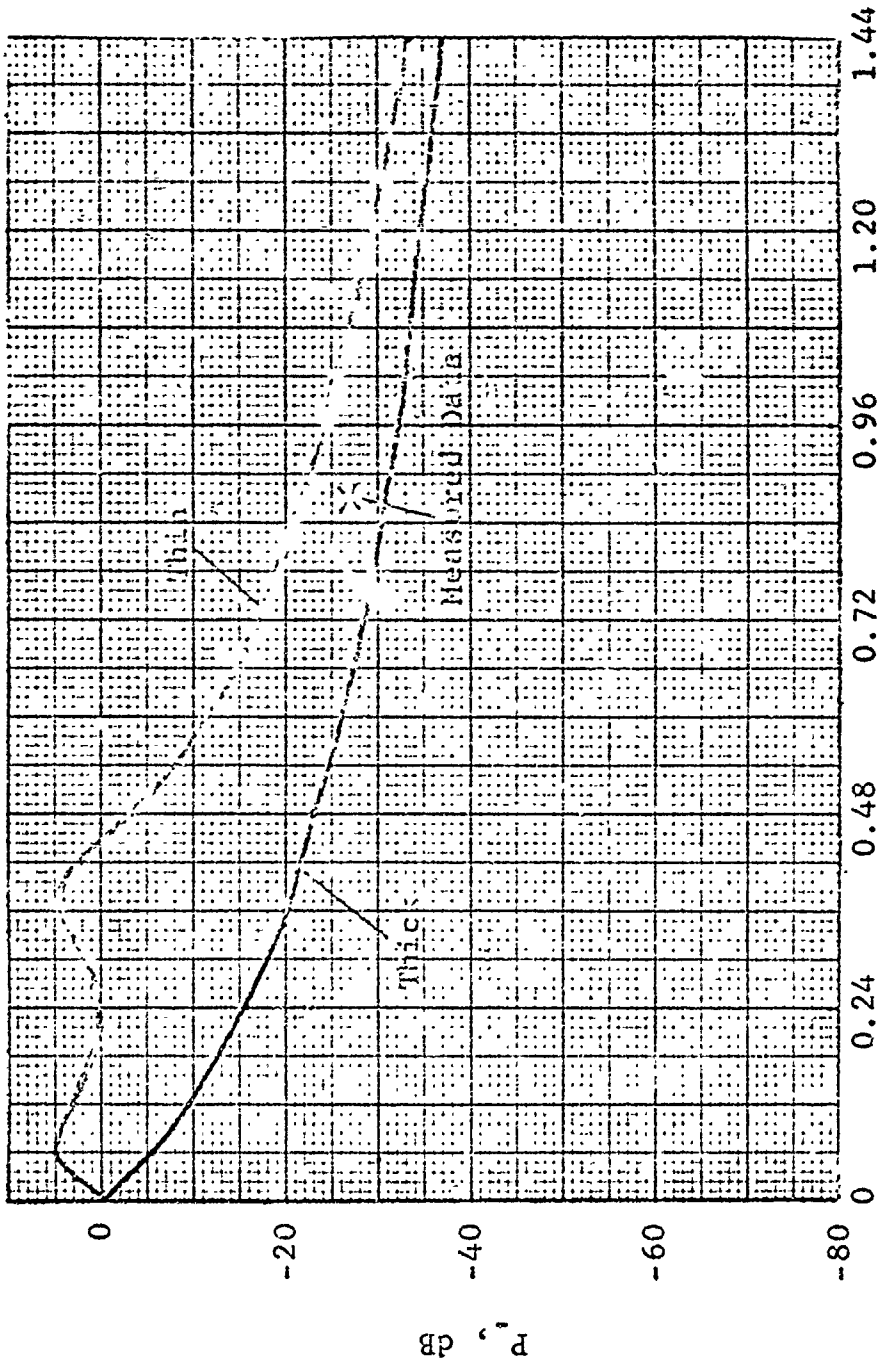


FIG. 15 - MEASURED AND COMPUTED DIFFERENCE FREQUENCY PRESSURE

The results in Figs. 5 through 8 are like those in Figs. 3 and 4 but for different dome-transducer spacings. The importance of these results is that they show the periodicity of $P_-$ with half wavelength increases in dome-transducer spacing. Furthermore, these results show that as $d$ is increased the difference in dB of $P_-$ between a resonant and antiresonant dome-transducer spacing decrease.

In Figs. 9 through 14, results are presented for a steering angle of $20^\circ$. For these off-axis cases, the standing wave patterns are different than for $\theta = 0^\circ$; hence, we do not see significant effects of cavity resonance, for the same values of $d$, as we did in Figs. 3 through 8. The main effects of changing impedance for this value of $\theta$ are seen for small dome thicknesses and are prominent in Figs. 10 and 13.

As previously stated, we were aware of only one piece of measured data available for comparison with our model, and this comparison is shown in Fig. 15 with appropriate parameters given in Table II. Nothing concrete can be said about our models or their predictive capability based on a comparison with one measured data point; however, it was encouraging to us that Konrad's measured point was bracketed by our two models.

## 6.0 CONCLUSIONS

1. Cavity resonances and material resonances are important effects affecting $P_-$.

2. For nonresonance conditions thick and thin model results agree very well for plate thicknesses much greater than $\lambda/10$.

3. For a velocity control transducer, if the impedance the transducer sees can be controlled by the dome-transducer spacing, then one can achieve more power out with a dome (under certain conditions) than with no-dome. The degree to which this effect would carry over into less idealized geometries is questionable however.

4. Our two models bracketed the one measured data point available to us.

5. The following calculating procedure is suggested as probably being adequate to make predictions of the influence of a dome upon the performance of parametric transmitting array:

1. Utilize existing linear dome programs in order to calculate the two primary fields at the dome's outer edge. This can be done both for thick and thin dome models.

2. Define the appropriate Green's function $\Gamma$ for the geometry at hand which satisfies the boundary condition at the dome's outer surface of $\Gamma = 0$.

3. An integral similar to that given in Eq. (25) can be set up. This will lead to the definition of an appropriate coefficient A which will be sensitive to the angle of incidence $\theta$, the frequencies involved, and the dome material parameters. Then the ratio of A (with dome) to A (without) can be calculated in order to gain insight into the

dome's effect upon the radiation field at the difference frequency. It should be emphasized that for three dimensional geometries this approach would reveal the dome's influence upon sidelobe structure in both the primary and secondary pressure fields as well as the efficiency of generation of $P_-$.

## 7.0 RECOMMENDATIONS

1. Simple experimental measurements need to be made to validate this model.

2. A parameter study should be carried out using current Navy window materials to identify those most useful for parametric arrays.

3. The concepts of this model should be analytically extended to more realistic geometries and experimentally verified in a small parallel measurement program.

## 8.0 ACKNOWLEDGEMENT

The authors wish to thank Earl MC Donald who carried out the numerical calculations.

TRACOR

## BIBLIOGRAPHY


1. R.E. Douglas, K.B. Hamilton, and R.F. Pohler, "Exploratory Development Dome Studies" Vol. II NAVSHIPS Contract NObsr-95349 (Code 00V1E) Tracor Document No. 67-917-U. October, 1967.

2. P.M. Morse and H. Feshbach, Methods of Theoretical Physics (McGraw-Hill Book Co., Inc. New York, N.Y., 1953), pp. 812-815.

3. L. Brekhovskikh, Waves in Layered Media (Academic Press, New York, N.Y.,1960), pp. 68-69.